Quasibound states of charged dilatonic black holes

Yang Huang[*] and Hongsheng Zhang[†]

School of Physics and Technology, University of Jinan, 336, West Road of Nan Xinzhuang, Jinan 250022, Shandong, China

(Received 23 December 2020; accepted 8 February 2021; published 26 February 2021)

Investigation of quasibound states of black holes is significant for expected ultralight particles, as well as black holes through gravitational waves. We first investigate quasibound states of a massive scalar field for dilatonic charged black holes via numerical analysis. We study the complex eigenfrequencies of the massive scalar field in a wide range of gravitational fine structure constant μM in detail, and show the effects of charge. Further, we study the eigenfrequencies of the massive field through an analytical approach by matching the near horizon solution and far field solution, and find its spectra for excited states by the iteration method. We demonstrate that the numerical solution and analytical solution perfectly agree with each other in the region where charge of the black hole is large, both for real and imaginary parts of the eigenfrequencies.

DOI: 10.1103/PhysRevD.103.044062

I. INTRODUCTION

Study of the bound system of the Sun and planets initiates classical mechanics, and study of the bound state of hydrogen atoms initiates quantum mechanics. With the discovery of gravitational waves and confirmation of black holes, bound state, scattering state, and quasinormal excitation take more and more significant status in black hole dynamics and astroparticle physics. Because of the distinctive properties of black holes, generally there are no real bound states for black holes, since any wave will infiltrate to the interior of the hole via quantum effects. The matter waves around a black hole will decay slowly or swiftly. Thus we call such state a quasibound state.

For astrophysical black holes, the mass of the quasibound particle is so tiny that it is difficult to observe at colliders or accelerators in terrestrial labs. For example, the axion, which is supposed to explain strong CP violation in QCD, is illusive in terrestrial labs, since its mass is expected to be 10^{-5} eV or much smaller [1,2]. Black holes present increasing prominence to probe ultralight particles. The particles around a hole may excite more similar ones if they have the proper frequencies. This type of radiation is a nonthermal one (superradiance), which is different from Hawking radiation. At the same time, the particles will leak into the black hole because of quantum tunneling. If the two processes get a detailed balance, the particles can form a "cloud" around a hole [3–8]. Through explorations of a high-resolution image of a black hole filmed by the Event Horizon Telescope, it expected to probe the ultralight bosonic particles based on the birefringent effects of electromagnetic waves [9].

Gravitational waves become a powerful probe to several dark astrophysical processes, which are difficult to see by traditional optical or electromagnetic observations, especially for the object which has no electromagnetic interaction, for example, dark matter. Nothing can escape from gravity interaction. The ultralight particles surrounding black holes imprint gravitational waves of black hole binaries. Actually, even a single gravitational-wave measurement can effectively sense the existence of ultralight bosons surrounding the gravitational wave source [10]. The observations of gravitational waves also reveal signals for bosonic clouds composed by the bound state of ultralight particles through spin-induced multipole moments and tidal Love numbers [11]. Recently, it is shown that one could find the signal of dark matter around black hole binary from gravitational tail wavelets [12].

Quasibound states of a black hole have been studied under several different conditions [13–23]. The minimal extension of general relativity, i.e., the dilatonic gravity or called scalar tensor theory, can be traced back to Kluza-Klein compactification and Dirac's large number hypothesis, in which only one new degree is introduced. The quasinormal modes of the charged dilatonic black hole is studied in Refs. [24,25]. The superradiant instability and charged scalar clouds of the dilatonic black hole is studied in Refs. [26–32]. Recently, the scattering properties of such a hole is studied in Ref. [33]. In this paper, we will discuss the quasibound state of a charged dilatonic black hole.

This paper is organized as follows. In the next section, we present the theory frame and our numerical method in detail. In Sec. III, we develop an analytical approach for the

[*]sps_huangy@ujn.edu.cn
[†]sps_zhanghs@ujn.edu.cn

complex eigenfrequency, especially for a black hole with large charge. In Sec. IV, we present our main result, and demonstrate that the results from the numerical method are well consistent with results from the analytical method, particularly in the case of large charge limit. In Sec. V, we concisely conclude this article.

II. MASSIVE SCALAR FIELD IN THE GMGHS SPACETIME

A. The background metric

The action of the four-dimensional Einstein-Maxwell-Dilaton theory is given by [34,35]

$$S = \int d^4x\sqrt{-g}[R - 2(\nabla\phi)^2 - e^{-2a\phi}F_{\mu\nu}F^{\mu\nu}], \quad (1)$$

where ϕ is the dilaton, and $F_{\mu\nu} = \partial_\mu A_\nu - \partial_\nu A_\mu$ is the Maxwell tensor. The coupling between the dilaton and the Maxwell field is governed by the parameter a. When $a = 0$, the action reduces to the Einstein-Maxwell action, while $a = 1$ corresponds to the low-energy limit of string theory. In this case, the static spherical charged black hole solution was first found by Gibbons and Maeda [34], and independently by Garfinkle, Horowitz, and Strominger [35] (GMGHS). In the Einstein frame, the line element of the GMGHS black hole is given by

$$ds^2 = -Fdt^2 + F^{-1}dr^2 + r^2G(d\vartheta^2 + \sin^2\vartheta d\varphi^2), \quad (2)$$

with

$$F(r) = 1 - \frac{2M}{r}, \quad \text{and} \quad G(r) = 1 - \frac{Q^2}{Mr}, \quad (3)$$

where M and Q are the mass and charge of the black hole, respectively. The Maxwell field and dilaton field read

$$F_M = Q\sin\vartheta d\vartheta \wedge d\varphi, \quad (4)$$

and

$$e^{-2\phi} = e^{-2\phi_0}\left(1 - \frac{Q^2}{Mr}\right), \quad (5)$$

respectively. ϕ_0 denotes the value of the dilaton ϕ at spacelike infinity. $\phi_0 = 0$ implies an asymptotic flat manifold. The event horizon of the GMGHS black hole is located at $r_+ = 2M$. The area of the sphere goes to zero when $r = r_- = Q^2/M$ and the surface is singular. For $Q < Q_{\max} \equiv \sqrt{2}M$, the singularity is enclosed by the event horizon. In the extremal case $Q = Q_{\max}$, and the singularity coincides with the horizon. Following Ref. [33], we introduce a normalized charge $q = Q/Q_{\max}$. To better manifest the behavior of quasibound state frequencies in the near extremal limit, we also parametrize the black hole charge by

$$q = 1 - e^{-\eta}. \quad (6)$$

Clearly, the black hole charge q increases monotonically with η. The Schwarzschild black hole corresponds to $\eta = 0(q = 0)$, while the extremal GMGHS black hole corresponds to $\eta \to \infty(q \to 1)$.

B. Massive Klein-Gordon equation

The massive Klein-Gordon equation governs a scalar field Φ of mass μ is $\nabla_\mu\nabla^\mu\Phi = \mu^2\Phi$. Decomposing the scalar field as $\Phi = e^{-i\omega t}R_{\omega l}(r)Y_{lm}(\vartheta,\varphi)$ yields the radial equation

$$\Delta\frac{d}{dr}\left(\Delta\frac{dR_{\omega l}}{dr}\right) + [G(r)^2\omega^2r^4 - U]R_{\omega l} = 0, \quad (7)$$

where

$$U = \Delta[l(l+1) + \mu^2r^2G(r)]. \quad (8)$$

It is useful to introduce a new radial function as

$$\psi_{\omega l}(r) = \frac{R_{\omega l}(r)}{r\sqrt{G(r)}}. \quad (9)$$

Then the radial equation becomes

$$\frac{d^2}{dx^2}\psi_{\omega l} + [\omega^2 - V_l(r)]\psi_{\omega l} = 0, \quad (10)$$

where $x = \int dr/F$ is the tortoise coordinate, and the effective potential is given by

$$V_l(r) = \frac{F(r)}{G(r)}\left[\frac{F'(r)}{r} + \frac{l(l+1)}{r^2} + \mu^2G(r)\right] - \frac{2M^2q^2}{r^4}\frac{F(r)}{G(r)^2}\left[1 + \frac{q^2}{2}\left(1 - \frac{6M}{r}\right)\right]. \quad (11)$$

Clearly, if we take $q = 0$, then $G(r) = 1$ and $V_l(r)$ reduces to the effective potential of the massive scalar field in the Schwarzschild spacetime. $q = 0$ also implies that the dilaton ϕ vanishes. Thus the dilaton ϕ is not an independent hair.

At the horizon, $V_l(r)$ vanishes for $q \neq 1$,[1] so the asymptotic solution to Eq. (10) is a superposition of ingoing and outgoing waves. Regularity requires a purely ingoing wave solution at the horizon,

$$\psi_{\omega l} \sim e^{-i\omega x} \sim (r - r_+)^{-2iM\omega}. \quad (12)$$

At infinity, the potential tends to μ^2, and the radial function has the following asymptotic behavior:

[1]We only consider the nonextremal case, i.e., $0 \leq q < 1$.

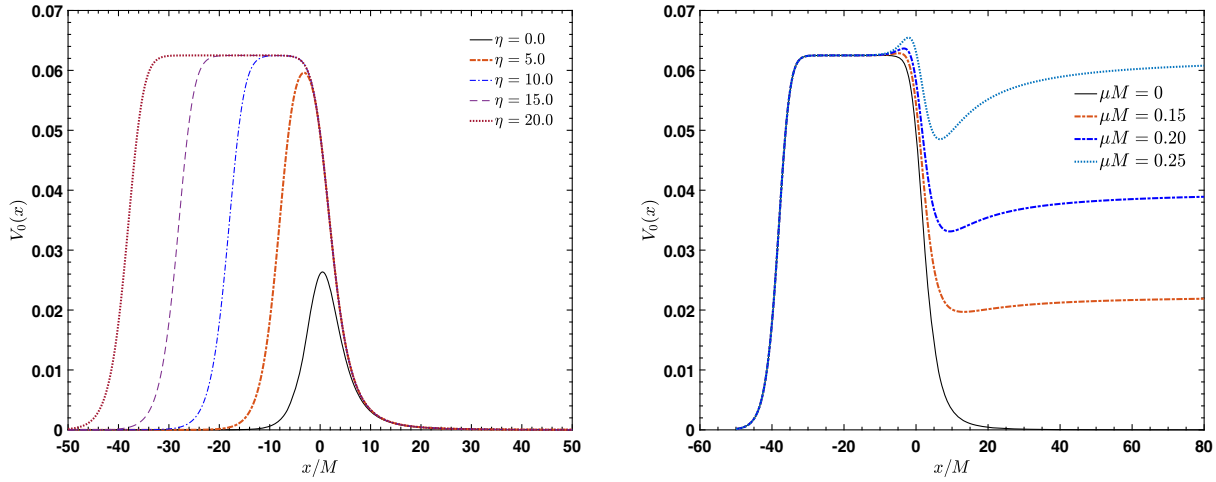

FIG. 1. Effective potential of $l = 0$ state as functions of x. In the left panel, we fix $\mu M = 0$ and compare the potential for different values of η, whereas in the right panel, we set $\eta = 20$ and compare the potential for different values of μM.

$$\psi_{\omega l} \sim r^{\chi} e^{\rho r}, \tag{13}$$

where

$$\chi = \frac{M(\mu^2 - 2\omega^2)}{\rho}, \quad \text{with} \quad \rho = \pm\sqrt{\mu^2 - \omega^2}. \tag{14}$$

The behavior of the radial function at large distance is determined by the sign of the real part of ρ. If $\mathrm{Re}(\rho) > 0$, the function is divergent, whereas if $\mathrm{Re}(\rho) < 0$, the function tends to zero. Here, we are interested in quasibound state solutions and choose $\mathrm{Re}(\rho) < 0$. Before proceeding, it would be helpful to analyze the behavior of the effective potential.

In Fig. 1, we present the potential of the $l = 0$ state, as a function of x. The left panel shows the effect of η on the potential. We fix $\mu M = 0$ and gradually increase the values of η. In the Schwarzschild case ($\eta = 0$), a potential barrier appears at $x/M \approx 0$; For $\eta < 5$ (or $q < 0.993$), both the height and width of the potential increase with η; Interestingly, when $\eta > 5$, the width continues to increase with η, while the height remains unchanged. In this case, the height of the potential is $(2l+1)^2/(16M^2)$.

To be more concrete, we define the width of the effective potential by $|x_2 - x_1|$, where $x_{1,2}$ are the tortoise coordinate, at which $V(x = x_{1,2}) = V_{\max}/2$, where $V_{\max}$ is the maximum value of the potential barrier. In Fig. 2, we present the width of the potential as a function of η. We see that the width is indeed increased monotonically with η. Especially, such growth is uniform when $\eta > 5$. Therefore, in the limit of $\eta \to \infty$, the GMGHS black hole becomes extremal and the potential barrier can be infinitely wide. This property is crucial for the existence of long-lived modes of massive scalar field adhered to a GMGHS black hole.

The right panel of Fig. 1 compares potentials for different values of μM. For $\mu M \neq 0$, the potential tends to μ^2 at infinity, and there is a potential well between the barrier and spatial infinity. A wave with $\omega < \mu$ will bounce back and forth in the well, leaking its energy to the black hole each time due to the tunneling effect of the potential barrier. Such a tunneling effect will be heavily suppressed in the near extremal limit $\eta \gg 1$, since the width of the potential barrier can be infinitely wide in this limit, as we have shown in the left panel in this figure. Thus, we expect that a surrounding massive scalar field could be notably long-lived for a near extremal GMGHS black hole.

C. Quasibound states

By imposing appropriate boundary conditions at the horizon and infinity, Eq. (10) defines an eigenvalue problem of ω. Solutions of Eq. (10) with boundary conditions (13) and (12) are called quasibound states of a massive scalar field. The two boundary conditions select a discrete set of complex frequencies (expressed by $\omega = \omega_R + i\omega_I$), which

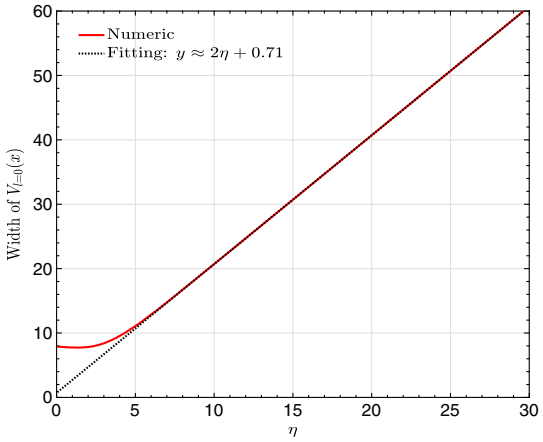

FIG. 2. Width of the effective potential with $l = 0$ as a function of η.

are called quasibound state frequencies. The unstable mode corresponds to $\omega_I > 0$, whereas $\omega_I < 0$ corresponds to the stable mode with an e-folding decaying timescale: $\tau = |\omega_I|^{-1}$.

Previous studies have shown that in the limit $\mu M \ll l$, the real part of the quasibound state frequency resembles that of the hydrogen atom

$$\omega_n \approx \left(1 - \frac{\mu^2 M^2}{2\tilde{n}^2}\right)\mu, \tag{15}$$

where $\tilde{n} = n + l + 1$ is the principal quantum number of the state. This formula also applies to the case of a massive scalar field around the GMGHS black hole.

In the following text, we shall derive a more accurate frequency spectrum of the quasibound states of a massive scalar field around the GMGHS black hole. More prominently, we shall show that the imaginary part of frequency tends to zero for a near extremal black hole ($\eta \to \infty$).

III. NUMERICAL METHOD

In this work, we apply the continued fraction method to compute the quasibound state frequencies. In Ref. [36], the authors have used this method to find the quasinormal modes of massive scalar field in Kerr-Sen black hole spacetime. In this article, we apply it under quite different boundary conditions at infinity.

As discussed in Sec. II, for quasibound states the radial function decays exponentially at infinity. Thus we may write the radial solution as

$$R_{\omega l}(r) = \left(\frac{r - r_+}{r - r_-}\right)^{-i\sigma}(r - r_-)^{\chi - 1}e^{\rho r} \times \sum_{n=0}^{\infty} a_n \left(\frac{r - r_+}{r - r_-}\right)^n, \tag{16}$$

where $\rho = -\sqrt{\mu^2 - \omega^2}$, $\chi = M(\mu^2 - 2\omega^2)/\rho$, and $\sigma = 2M\omega$. Substituting this equation into Eq. (7) yields a three-term recurrence relation among the expansion coefficients a_n,

$$\alpha_0 a_1 + \beta_0 a_0 = 0, \tag{17a}$$

$$\alpha_n a_{n+1} + \beta_n a_n + \gamma_n a_{n-1} = 0, \quad \text{for } n > 0, \tag{17b}$$

where α_n, β_n and γ_n are, respectively, given by

$$\alpha_n = (1 + n)(1 + n - 4i\omega), \tag{18}$$

$$\beta_n = -2n^2 - 2\left[1 - 4i\omega + (2q^2 - 3)\rho + \frac{\omega^2}{\rho}\right]n - l(l+1) - (1 - 4i\omega)\left[1 + (2q^2 - 3)\rho + \frac{\omega^2}{\rho}\right] + 8\omega^2 + 4(1 - q^2)(2\omega^2 - \mu^2), \tag{19}$$

and

$$\gamma_n = n^2 - 4i\omega n - 8\omega^2 + \frac{2(n - 2i\omega)(2\omega^2 - \mu^2)}{\rho} + \frac{\mu^4}{\rho^2}. \tag{20}$$

Here, we set $M = 1$, and all other quantities are measured by M. Then, the quasibound state frequencies are obtained by solving numerically the following equation [37]:

$$0 = \beta_0 - \frac{\alpha_0\gamma_1}{\beta_1 -}\frac{\alpha_1\gamma_2}{\beta_2 -}\frac{\alpha_2\gamma_3}{\beta_3 -}\cdots. \tag{21}$$

IV. ANALYTICAL METHOD

In the near-extremal limit ($q \to 1$), the eigenvalue problem introduced in the previous section can be solved analytically. It is convenient to introduce the following dimensionless quantities

$$z \equiv \frac{r - r_+}{r_+}; \qquad \tau \equiv \frac{r_+ - r_-}{r_+} = 1 - q^2. \tag{22}$$

Then, the radial equation (7) becomes

$$z(z + \tau)\frac{d^2R}{dz^2} + (2z + \tau)\frac{dR}{dz} + VR = 0, \tag{23}$$

with

$$V = \frac{4\tau\epsilon^2}{z} - l(l+1) + 4(1 + 2\tau)\epsilon^2 - 4\tau\mu_s^2 + 4[\epsilon^2 + (1 + \tau)(\epsilon^2 - \mu_s^2)]z + 4(\epsilon^2 - \mu_s^2)z^2. \tag{24}$$

where $\epsilon = \omega M$ and $\mu_s = \mu M$ are the dimensionless frequency and mass, respectively.

A. Near horizon solution

Close to the event horizon $z \to 0$, we can omit higher order terms of z. Hence, Eq. (23) becomes

$$z(z + \tau)\frac{d^2R}{dz^2} + (2z + \tau)\frac{dR}{dz} + \left(\frac{4\tau\epsilon^2}{z} + \frac{1}{4} - \beta^2\right)R = 0, \tag{25}$$

where

$$\beta^2 = \left(l + \frac{1}{2}\right)^2 + 4\tau\mu_s^2 - 4(1 + 2\tau)\epsilon^2. \tag{26}$$

The ingoing wave solution of Eq. (25) is

$$R(z) \sim \left(\frac{z}{\tau}\right)^{-2i\epsilon}{}_2F_1\left(\frac{1}{2} - \beta - 2i\epsilon, \frac{1}{2} + \beta - 2i\epsilon; 1 - 4i\epsilon; -\frac{z}{\tau}\right), \tag{27}$$

where ${}_2F_1(a,b;c;z)$ is the hypergeometric function. Considering the limit $z \gg \tau$, and using the property of the hypergeometric function

$$ {}_2F_1(a,b;c;z) = \frac{\Gamma(c)\Gamma(b-a)}{\Gamma(c-a)\Gamma(b)} u_3 + \frac{\Gamma(c)\Gamma(a-b)}{\Gamma(c-b)\Gamma(a)} u_4, \tag{28} $$

where

$$ u_3 = (-z)^{-a} {}_2F_1\left(a, a+1-c; a+1-b; \frac{1}{z}\right), \tag{29a} $$

$$ u_4 = (-z)^{-b} {}_2F_1\left(b, b+1-c; b+1-a; \frac{1}{z}\right), \tag{29b} $$

the near horizon solution can be written as

$$ R(z) \sim \frac{\Gamma(1-4i\epsilon)\Gamma(2\beta)}{\Gamma(\frac{1}{2}+\beta-2i\epsilon)^2} \left(\frac{z}{\tau}\right)^{-\frac{1}{2}+\beta} + (\beta \to -\beta). \tag{30} $$

Here the second term $(\beta \to -\beta)$ refers to a replacement of β with $-\beta$ of the first term.

B. Far region solution

Now we consider the far region solution of the radial equation. For $z \gg \tau$, Eq. (23) becomes

$$ z^2 \frac{d^2R}{dz^2} + 2z\frac{dR}{dz} + \left[\frac{1}{4} - \beta^2 + 2\kappa k z - k^2 z^2\right] R = 0, \tag{31} $$

where β is given in Eq. (26), and

$$ \kappa = \frac{4\epsilon^2 - (1+\tau)k^2}{2k}, \tag{32} $$

with $k = 2\sqrt{\mu_s^2 - \epsilon^2}$. The solution of Eq. (31) is

$$ R(z) = C_1 e^{-kz} (2k)^{\frac{1}{2}+\beta} z^{-\frac{1}{2}+\beta} M\left(\frac{1}{2}+\beta-\kappa, 1+2\beta, 2kz\right) + C_2 \times (\beta \to -\beta), \tag{33} $$

where $M(a,c,z)$ is the confluent hypergeometric function, and $\{C_1, C_2\}$ are constants to be determined by the matching and boundary conditions. For $z \gg 1$, the confluent hypergeometric function behaves as

$$ M(a,c,z) \sim \frac{\Gamma(c)}{\Gamma(a)} e^z z^{a-c} + \frac{\Gamma(c)}{\Gamma(c-a)} (-1)^a z^{-a}. \tag{34} $$

Hence, for $z \gg 1$, the far region solution (33) reduces to

$$ \begin{aligned} R(z \to \infty) \sim & \left[C_1 \frac{\Gamma(1+2\beta)}{\Gamma(\frac{1}{2}+\beta-\kappa)} + C_2 \times (\beta \to -\beta)\right] \times (2k)^{-\kappa} z^{-1-\kappa} e^{kz} \\ & + \left[C_1 \frac{\Gamma(1+2\beta)}{\Gamma(\frac{1}{2}+\beta+\kappa)} (2k)^{\kappa} z^{-1+\kappa} (-1)^{\frac{1}{2}+\beta-\kappa} \right. \\ & \left. + C_2 \times (\beta \to -\beta)\right] e^{-kz}. \end{aligned} \tag{35} $$

For quasibound states, the radial function tends to zero at infinity. Therefore, the coefficient of the first term in Eq. (35) equals to zero,

$$ C_1 \frac{\Gamma(1+2\beta)}{\Gamma(\frac{1}{2}+\beta-\kappa)} + C_2 \times (\beta \to -\beta) = 0. \tag{36} $$

C. Matching the two solutions

For near extremal GMGHS black holes with $\tau \ll 1$, there is an overlap region $\tau \ll z \ll 1$ in which the two solutions should match each other. We have obtained the $z \gg \tau$ behavior of the near horizon solution, see Eq. (30). On the other hand, the $z \ll 1$ limit of the far region solution (33) is

$$ R(z) \sim C_1 (2k)^{\frac{1}{2}+\beta} z^{-\frac{1}{2}+\beta} + C_2 \times (\beta \to -\beta). \tag{37} $$

Comparing this equation with Eq. (30), we obtain

$$ C_1(\beta) = \left(\frac{\tau}{2k}\right)^{1/2} \frac{\Gamma(1-4i\epsilon)\Gamma(+2\beta)}{\Gamma(\frac{1}{2}+\beta-2i\epsilon)^2} (2k\tau)^{-\beta}, \quad \text{and} \quad C_2(\beta) = C_1(-\beta). \tag{38} $$

Substituting this equation into Eq. (36), we have

$$ \frac{\Gamma(\frac{1}{2}-\beta-\kappa)}{\Gamma(\frac{1}{2}+\beta-\kappa)} = \frac{\Gamma(\frac{1}{2}+\beta-2i\epsilon)^2\Gamma(-2\beta)^2}{\Gamma(\frac{1}{2}-\beta-2i\epsilon)^2\Gamma(+2\beta)^2} (2k\tau)^{2\beta}. \tag{39} $$

This is the equation of the quasibound state frequency in the near extremal limit. For given values of $\{l, \mu, \tau\}$, we compute the eigenvalues of ϵ by solving Eq. (39) numerically. If $\epsilon < \mu_s < L/2$, this equation can also be solved iteratively. For $\tau \ll 1$, the right-hand side of Eq. (39) is very small. Therefore, we obtain the approximation of ϵ by requiring that the left-hand side equals to zero. Using the property of the Gamma function $1/\Gamma(-n) = 0$, we have

$$ \frac{1}{2} + \beta - \kappa = -n. \tag{40} $$

This equation can be solved by assuming

$$\epsilon = \mu_s \left[1 + \sum_{i=1}^{\infty} C_i \mu_s^{2i} \right]. \tag{41}$$

Substituting Eq. (41) into Eq. (40), the coefficients C_i can be solved order by order for arbitrary i. Here we list the first third C_i:

$$C_1 = -\frac{1}{2\tilde{n}^2}, \tag{42a}$$

$$C_2 = -\frac{2(1+\tau)}{\tilde{n}^3 L} + \frac{\tau + 15/8}{\tilde{n}^4}, \tag{42b}$$

$$C_3 = -\frac{2(1+\tau)^2}{\tilde{n}^3 L^3} + \frac{6(\tau+1)^2}{\tilde{n}^4 L^2} \tag{42c}$$

$$+ \frac{8\tau^2 + 27\tau + 17}{\tilde{n}^5 L} - \frac{40\tau^2 + 152\tau + 145}{16\tilde{n}^6}, \tag{42d}$$

where $\tilde{n} = n + l + 1$ and $L = l + 1/2$. For long-lived modes with $\omega_I \ll \omega_R$, Eq. (41) may be treated as an approximation of the real part ω_R. Clearly, in the small mass limit $\mu_s \ll 1$, we can omit C_i for $i \geq 2$, and recover the hydrogenic spectrum, see Eq. (15). However, if μ_s is comparable to L, i.e., $\mu_s \lesssim L/2$, it is necessary to consider higher order terms to get more accurate results.

Comparing to the real part, we derive the imaginary part via a different way. The imaginary part ω_I can be obtained perturbatively. Substituting $\epsilon = \omega_R + i\omega_I$ into Eq. (39), we obtain the equation for ω_I. Then, we treat both ω_I and the right-hand side of Eq. (39) as small numbers, and expand the equation in terms of ω_I. Finally, we obtain the approximation of ω_I by letting the linear part of the expansion equal to zero. The whole procedure is tediously lengthy, and the resulting formula is too cumbersome to be presented here. In brief, we find

$$\omega_I M \propto -e^{-2\tilde{\beta}\eta}, \tag{43}$$

where η is defined in Eq. (6) and

$$\tilde{\beta} = \sqrt{\left(l + \frac{1}{2}\right)^2 - 4\omega_R^2}. \tag{44}$$

V. RESULTS

In this section, we systematically demonstrate our numerical and analytical results of the frequencies of quasibound states, both for ground states and excited states. Significantly, we find that the numerical results agree well with the analytical results, especially for near extremal black holes.

First, we show the complex frequencies of the ground quasibound state of the GMGHS black hole with different charges varies with respect to fine structure constants μM. Figure 3 compares the spectra of $l = 0$ states for different values of black hole charge q. Here, the Schwarzschild case ($q = 0$) is also plotted in comparison. For a very small fine structure constant $\mu M \ll 1$, the Compton wavelength of the scalar field is much larger than the size of the black hole. In this case, the real part of the frequency is well described by Eq. (15), and the effect of q is negligible. Physically, a very long wave hardly senses the existence of charge. Similar phenomena appear in scattering of GMGHS black holes and Reissner-Nordstrom black holes [33]. As the mass coupling μM is increased, the effect of q on ω_R becomes significant. The physical explanation is that a shorter wavelength yields a smaller expectation of spatial radius of the wave function, which implies that the surrounding massive particle is nearer to the central black hole than the weak coupling case. The gravitational effect of the charge decreases with respect to r much faster than that of the mass. Thus for a neutral particle far away from a charged mass point, it almost does not sense the gravity of charge. But when it is put nearer and nearer to the charged mass point, the gravity effects of the charge of the hole become more and more evident.

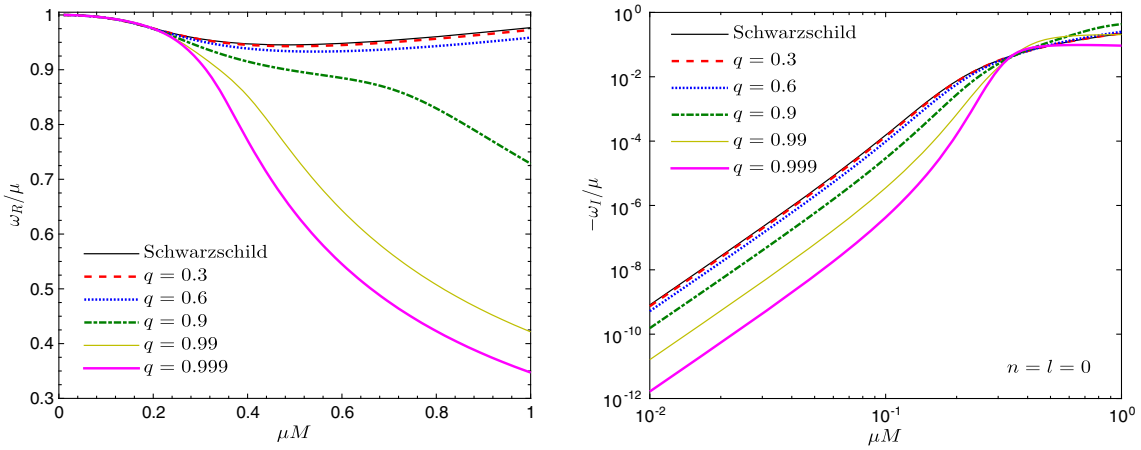

FIG. 3. The frequencies of the ground quasibound state of the $l = 0$ state as functions of μM. The left panel shows the real part ω_R, whereas the right panel shows the corresponding lines for the imaginary part ω_I.

As for the imaginary part of the frequency, the effect of q is significant, even in the limit $\mu M \ll 1$. From the right panel of Fig. 3, we see that for a given value of μM, $|\omega_I|$ decreases with the increase of q. Such trends are more notable in the near extremal limit. For example, when $\mu M = 0.2$, the value of $|\omega_I|$ for $q = 0.9$ is about 4 times that for $q = 0.99$; And the value of $|\omega_I|$ for $q = 0.99$ is again about 4 times that for $q = 0.999$, whereas the increase of q is only one-tenth of the former case. Physically, from Fig. 1 it is clear that a larger q leads to a wider potential. A wider potential is more difficult to penetrate, which is equal to say a smaller imaginary part of the frequency.

In Fig. 4, we present energy spectra for different angular momentum l. This figure shows that for small values of μM, the real part of the frequency is well approximated by Eq. (15), and the imaginary part ω_I tends to zero in the limit

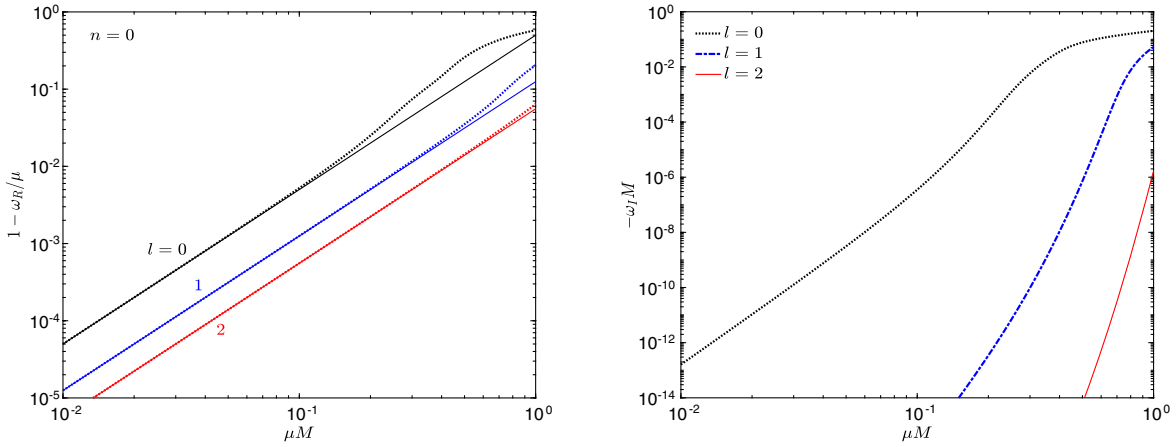

FIG. 4. Spectra of the quasibound states, with $n = 0$, for $l = 0$, 1, and 2. The black hole charge is $q = 0.99$. The left panel shows the real part ω_R (or more precisely $1 - \omega_R/\mu$), whereas the right panel shows the corresponding lines for the imaginary part ω_I. In the left panel, the dashed lines denote numerical results, whereas the solid lines denote the analytic results; see Eq. (15).

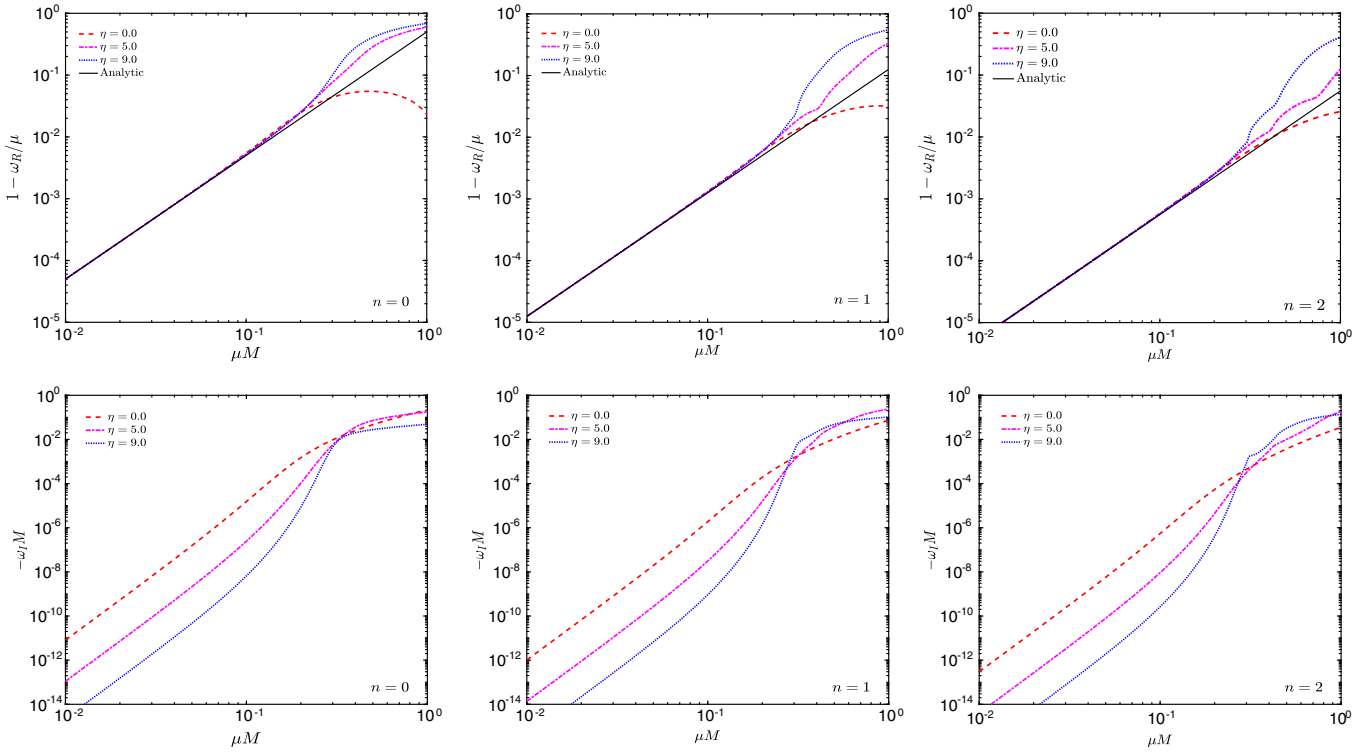

FIG. 5. Spectra of $l = 0$ state for different values of η. The upper panel shows the real part ω_R (or more precisely $1 - \omega_R/\mu$), whereas the bottom panel shows the corresponding lines for the imaginary part ω_I. The analytical result in this figure is given by Eq. (15). The excitation number $n = 0$, 1, and 2 for the left, middle, and right panels, respectively.

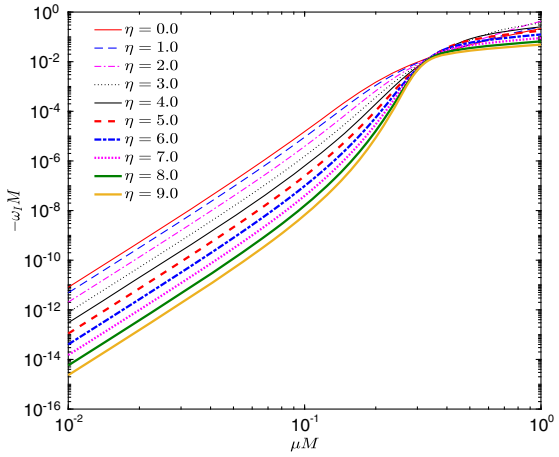

FIG. 6. Imaginary part of the quasibound state frequencies, with $n = l = 0$, as a function of μM for different values of η.

$\mu M \ll 1$. This means that the ultralight scalar field can be very long-lived around the GMGHS black hole. Similar results have been found for massive scalar and Dirac fields around a Schwarzschild or a Reissner-Nordström black hole [17,22,23].

From the analysis in Sec. II B, we expect that ω_I tends to zero in the extremal limit. Figure 5 compares the spectra of $l = 0$ state for different values of η. The upper panel shows more clearly that the real part of the frequency of the quasibound states with the same value of $\tilde{n} = n + l + 1$ degenerate in the limit $\mu M \ll 1$ and such degeneracy does not depend on the black hole charge, as predicted by Eq. (15). From Eqs. (41) and (42), the parameter η only affects ω_R when the coupling constant μM is comparable to L. The effects of η on ω_I is much more notable. We see that for a given μM, $|\omega_I|$ decreases with the increase of η. This confirms our physical analysis from Fig. 3.

In Fig. 6, we compare the imaginary part of the frequency of the ground state (with $n = l = 0$) for different values of η. The plot shows again that $|\omega_I|$ decreases with the increase of the black hole charge. We find that for $\mu M < 0.25$ the logarithm of $|\omega_I|$ almost decreases uniformly as η increases. This means that $|\omega_I|$ swiftly goes to zero in the limit $\eta \to \infty$.

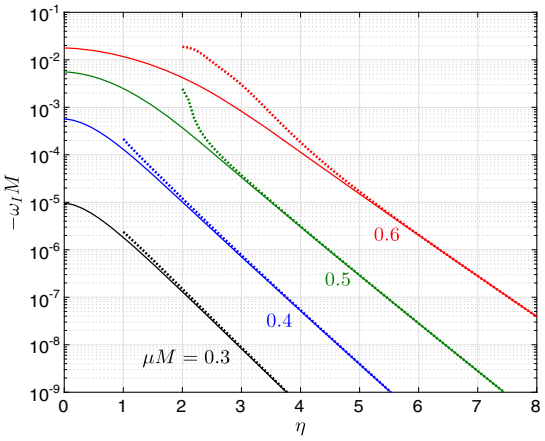

FIG. 8. The lowest quasibound state frequencies of the $l = 1$ state as functions of η, for $\mu M = 0.3, 0.4, 0.5, 0.6$. The solid lines denote the numerical results, while the dashed lines denote the analytical results obtained from Eq. (39).

In Fig. 7, we show the quasibound state frequencies of $l = 0$ state as functions of η, for different values of μM. For both the real and imaginary parts of the frequency, numerical results agree quite well with the analytical ones, especially for large value of η. As expected, the imaginary part $|\omega_I|$ tends to zero exponentially.

Figure 8 compares the imaginary part of the frequencies of $l = 1$ state for different values of μM. Again, we see that $|\omega_I|$ tends to zero exponentially at large η. For lower mass coupling μM, $|\omega_I|$ goes down faster. A smaller coupling μM implies a larger Compton wavelength, which denotes a larger expectation of r for the wave function. And a lower probability of tunneling follows a smaller

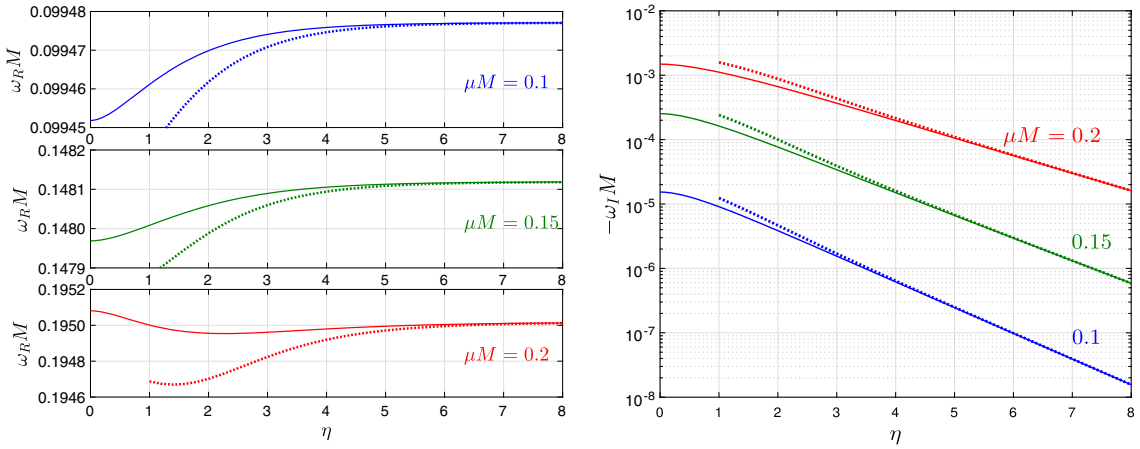

FIG. 7. The lowest quasibound state frequencies of $l = 0$ state as functions of η, for $\mu M = 0.1, 0.15, 0.2$. The left panel shows the real part ω_R of the frequency, and the right panel shows the imaginary part (or more precisely, $|\omega_I|$). In this plot, the solid lines denote the numerical results, while the dashed lines denote the analytical results obtained from Eq. (39).

coupling μM, that is to say a smaller imaginary part of the eigenfrequency.

VI. DISCUSSION AND CONCLUSION

The bound state of the hydrogen atom has fundamental importance, not only for quantization of matter, but also for quantization of electromagnetic field. Through transition between different energy levels, one directly demonstrates that the electromagnetic field is quantized. As it is well known, the quantization of gravity is a long-standing problem. A main reason why a full-fledged quantum gravity theory is still in absence is that we have no guide to develop such a theory from lab experiments or astrophysical observations. Similar to the case of the hydrogen atom, the transition between different energy levels of the (quasi)bound state should emit or absorb gravitons, i.e., a gravitational wave at a given frequency. It is very difficult, if not impossible, to detect the quantum property of gravitational waves from binary black holes [38–40]. The transition between different energy levels of the quasibound state of a black hole leave fingerprints in the gravitational wave signals, if the progenitors of the wave have surrounding bounded articles. It may be beneficial to probe the quantum property of the gravity field through analysis of gravitational waves from such progenitors.

The GMGHS black hole is a charged solution in dilatonic gravity. Dilatonic gravity is a minimal extension of general relativity, in which a new dilaton degree is introduced. The GMGSH solution is not a hairy black hole, since the dilatonic charge is determined by the electromagnetic charge. Thus the dilatonic charge is not an independent new charge.

In this article, we study the quasibound state of massive scalar fields in the GMGHS black hole spacetime. We computed the eigenfrequencies of the quasibound state via both analytical and numerical method. Results obtained from the two approaches finely agree with each other.

We found that in the extremal limit $\eta \to \infty$ (or $q \to 1$), the imaginary part of the frequency tends to zero exponentially. This implies that massive scalar field configurations around a near extremal GMGHS black hole may be notably long-lived.

ACKNOWLEDGMENTS

We thank Dao-Jun Liu for helpful discussions. This work is supported by the National Key Research and Development Program of China (No. 2020YFC2201400), as well as Shandong Province Natural Science Foundation under Grant No. ZR201709220395.

[1] V. B. Klaer and G. D. Moore, J. Cosmol. Astropart. Phys. 11 (2017) 049.
[2] D. J. E. Marsh, Phys. Rep. **643**, 1 (2016).
[3] R. Penrose and R. Floyd, Nature (London) **229**, 177 (1971).
[4] W. H. Press and S. A. Teukolsky, Nature (London) **238**, 211 (1972).
[5] W. H. Press and S. A. Teukolsky, Astrophys. J. **185**, 649 (1973).
[6] S. Teukolsky and W. Press, Astrophys. J. **193**, 443 (1974).
[7] S. Hod, Phys. Rev. D **90**, 024051 (2014).
[8] C. A. R. Herdeiro and E. Radu, Phys. Rev. Lett. **112**, 221101 (2014).
[9] Y. Chen, J. Shu, X. Xue, Q. Yuan, and Y. Zhao, Phys. Rev. Lett. **124**, 061102 (2020).
[10] O. A. Hannuksela, K. W. Wong, R. Brito, E. Berti, and T. G. Li, Nat. Astron. **3**, 447 (2019).
[11] D. Baumann, H. S. Chia, and R. A. Porto, Phys. Rev. D **99**, 044001 (2019).
[12] K. Lin, W.-L. Qian, X. Fan, and H. Zhang, Chin. Phys. C **44**, 071001 (2020).
[13] R. Cayuso, O. J. Dias, F. Gray, D. Kubizňák, A. Margalit, J. E. Santos, R. Gomes Souza, and L. Thiele, J. High Energy Phys. 04 (2020) 159.
[14] X. Qiao, M. Wang, Q. Pan, and J. Jing, Eur. Phys. J. C **80**, 509 (2020).
[15] P. Li, Y. Huang, C.-J. Feng, and X.-Z. Li, Phys. Rev. D **102**, 024063 (2020).
[16] Y. Huang, D.-J. Liu, X.-h. Zhai, and X.-z. Li, Phys. Rev. D **98**, 025021 (2018).
[17] Y. Huang, D.-J. Liu, X.-h. Zhai, and X.-z. Li, Phys. Rev. D **96**, 065002 (2017).
[18] Y. Huang, D.-J. Liu, and X.-Z. Li, Int. J. Mod. Phys. D **26**, 1750141 (2017).
[19] Y. Huang and D.-J. Liu, Phys. Rev. D **94**, 064030 (2016).
[20] S. L. Detweiler, Phys. Rev. D **22**, 2323 (1980).
[21] H. Furuhashi and Y. Nambu, Prog. Theor. Phys. **112**, 983 (2004).
[22] X.-N. Zhou, X.-L. Du, K. Yang, and Y.-X. Liu, Phys. Rev. D **89**, 043006 (2014).
[23] J. Barranco, A. Bernal, J. C. Degollado, A. Diez-Tejedor, M. Megevand, M. Alcubierre, D. Nunez, and O. Sarbach, Phys. Rev. Lett. **109**, 081102 (2012).
[24] V. Ferrari, M. Pauri, and F. Piazza, Phys. Rev. D **63**, 064009 (2001).
[25] X.-Z. Li, J.-G. Hao, and D.-J. Liu, Phys. Lett. B **507**, 312 (2001).
[26] Y. Huang, D.-J. Liu, X.-H. Zhai, and X.-Z. Li, Classical Quantum Gravity **34**, 155002 (2017).
[27] H. M. Siahaan, Int. J. Mod. Phys. D **24**, 1550102 (2015).
[28] C. Bernard, Phys. Rev. D **94**, 085007 (2016).

[29] C. Bernard, Phys. Rev. D **96**, 105025 (2017).
[30] R. Li, Phys. Rev. D **88**, 127901 (2013).
[31] R. Li, J. Zhao, X. Wu, and Y. Zhang, Eur. Phys. J. C **75**, 142 (2015).
[32] R. Li and J. Zhao, Phys. Lett. B **740**, 317 (2015).
[33] Y. Huang and H. Zhang, Eur. Phys. J. C **80**, 654 (2020).
[34] G. W. Gibbons and K.-i. Maeda, Nucl. Phys. **B298**, 741 (1988).
[35] D. Garfinkle, G. T. Horowitz, and A. Strominger, Phys. Rev. D **43**, 3140 (1991); **45**, 3888(E) (1992).
[36] K. D. Kokkotas, R. A. Konoplya, and A. Zhidenko, Phys. Rev. D **92**, 064022 (2015).
[37] E. W. Leaver, Proc. R. Soc. A **402**, 285 (1985).
[38] F. Dyson, Int. J. Mod. Phys. A **28**, 1330041 (2013).
[39] M. Parikh, F. Wilczek, and G. Zahariade, Int. J. Mod. Phys. D **29**, 2042001 (2020).
[40] Z. Hongsheng and F. Xilong, arXiv:1809.06511.